

# Walking dynamics are symmetric (enough)

M. Mert Ankaralı, Shahin Sefati, Manu S. Madhav, Andrew Long, Amy J. Bastian, and Noah J. Cowan

## Abstract

Many biological phenomena, such as locomotion, circadian cycles, and breathing are quasi-periodic in nature and can be modeled as rhythmic dynamical systems. Dynamical systems modeling often involves neglecting certain characteristics of a physical system as a modeling convenience. For example, in the dynamics of locomotion, the musculoskeletal system is commonly treated as symmetric about the sagittal plane. Here we extend statistical cross validation techniques in order to examine the consequences of assuming (or not) bilateral symmetry. Indeed, we verify that there are statistically significant asymmetries in the dynamics of human walking, but nevertheless show that ignoring these asymmetries results in a more consistent and predictive model. In general, neglecting evident characteristics of a system can be more than a modeling convenience—it can produce a better model.

## I. INTRODUCTION

The concept of symmetry has helped shape our understanding of engineering and biology alike. The Roman text “De architectura” by Vitruvius and the eponymous “Vitruvian Man” by Leonardo Da Vinci exemplify the influence of symmetry in animals and humans on man-made works of art and engineering. Symmetry serves to simplify and reduce complexity, making it a powerful tool in computational and analytical applications. The ubiquity of bilateral (left–right, sagittal plane) symmetry in animals is genetically encoded [1], and from an engineering point of view, building machines with bilateral symmetry is justified by the fact that the left–right axis is unbiased either by gravity or by direction of movement. However, genetic encoding of symmetry manifests itself imperfectly: numerous factors, such as differences in contralateral limb lengths, dominance of “leggedness” and handedness, and developmental processes break perfect symmetry, and enhance asymmetry.

Several parameters of human [2–5] and non-human [6, 7] locomotion have been quantified as being bilaterally symmetric, and this is thought to confer some advantages on motor abilities (e.g. reduced energy cost [8]). However, these studies examined steady state and/or kinematic symmetry, i.e. symmetry of limb lengths, topology of gait patterns, ground reaction forces, stride lengths, and other kinematic parameters. More importantly, they did not examine the potential benefits of neglecting asymmetry. For example, during human walking, do steps from left-to-right and right-to-left recover significantly differently from perturbations? Indeed there are differences in leg

M. Mert Ankaralı, Shahin Sefati, Manu S. Madhav and Noah J. Cowan are with the Dept. of Mechanical Eng., Johns Hopkins University, 21218 Baltimore, MD, USA [mertankarali@jhu.edu](mailto:mertankarali@jhu.edu)

Andrew Long is with the Dept. of Biomedical Eng., Johns Hopkins University, 21218 Baltimore, MD, USA

Amy J. Bastian is with the Dept. of Neuroscience, Johns Hopkins University, 21218 Baltimore, MD, USA

“dominance”—e.g. preferred kicking leg—which might lead to different responses from step-to-step. If there is a step-to-step dynamical asymmetry, does fitting a model from stride to stride (two step) rather than step to step (one step) better capture the dynamics of human walking. Indeed there is no single physical system with perfect “symmetry”. Thus symmetric models are inherently wrong for any physical system, but may nevertheless be useful for simplifying both the modeling and analysis.

“Essentially all models are wrong, but some are useful” wrote George E. P. Box in his seminal book [9]. According to Box, the important practical concern regarding the models of physical phenomena is “how wrong do they have to be to not be useful?” With regard to bilateral asymmetry in human walking, we attempt to frame this concern as follows. How wrong is it to neglect asymmetry from a statistical point of view? And how useful is symmetric modeling in terms of predictive power and simplicity? In most cases correctness and usefulness are directly related and they are tested simultaneously. However in the context of data-driven modeling of human walking dynamics, the “wrongness” and “usefulness” of assuming symmetry are related but have critical, nuanced differences. The methods presented in this paper allows us to independently (statistically) address these differences.

In this paper, we extend classical cross-validation techniques to test the assumption of bilateral symmetry in the dynamics of human walking. For example, we fit Poincaré return maps to “left steps” and “right steps” and tested these maps in terms of their respective ability to predict just the left-step dynamics. If walking were perfectly symmetric, both types of return maps would perform identically in left-step cross validation. However, we show that there are indeed statistically significant asymmetries in the dynamics of human walking. Despite these asymmetries we show that a more consistent and predictive model of the dynamics is obtained by assuming symmetry, pooling all the data from both left steps and right steps to form a generic step map. Quite surprisingly, this fit significantly out-performs the mapping fitted to only left steps even when predicting left step data. Moreover, it is theoretically convenient to assume symmetry. These advantages lead us to conclude that the assumption of symmetry in walking dynamics, though clearly wrong in a platonic sense, is nevertheless more useful for all practical purposes.

### *A. Modeling the Rhythmic Dynamics*

Our approach to analyzing and modeling walking involves treating the underlying behavior as a finite-dimensional nonlinear rhythmic dynamical system operating around a stable limit cycle. This type of modeling approach has been successful for robotic [10–12] and biological systems [13–15]. A limit cycle is an isolated periodic trajectory which is a solution to the equations governing the dynamical system [16]. A limit cycle is said to be stable if all trajectories in a sufficiently small neighborhood of the limit cycle converge to it.

We further use Poincaré theory in our analysis of rhythmic walking dynamics. A Poincaré return map [14, 16] is a mapping from a transverse section  $S$  back to itself, obtained by tracing the consecutive intersections of the state trajectories with the section  $S$ . This return map reduces the continuous rhythmic dynamical system to a nonlinear discrete dynamical system that preserves many properties of the behavior. The specific Poincaré section that we adopt for human walking is heel strike, as explained in Section II-B.

The intersection of the limit cycle with the Poincaré section is an isolated fixed point of the return map. The limit

cycle is asymptotically stable if and only if this fixed point is stable. Our second modeling approximation is based on the Hartman-Grobman theorem (or linearization theorem), which states that local flow around any hyperbolic fixed point is homeomorphic to the one governed by its linearization around the fixed point itself. Thus as detailed in Section II-B, we fit linear models to walking trajectories on the Poincaré maps.

### B. Limit-Cycle Dynamics and Symmetry

Here, we define symmetry in the context of limit-cycle modeling of walking and consider what kind of symmetries (and asymmetries) can be addressed using this approach.

In our modeling approach there are two core elements: the limit-cycle of the rhythmic system which characterizes the steady-state behavior, and the dynamics (both deterministic and stochastic) around the limit-cycle. In this paper we are interested in the latter.

Beyond its utility for approximation, bilateral symmetry of the (steady-state) limit cycle trajectory may have physiological significance, such as reducing metabolic cost [8, 17]. Indeed the majority of studies that address human or animal locomotor symmetry focus on symmetry of steady-state variables and parameters such as ground reaction forces and gait patterns [2–4, 6, 7] and thus implicitly approach the problem from the limit-cycle perspective.

Here, we consider the dynamics near, but *off of* the limit cycle, using data from Poincaré sections to estimate Poincaré maps. To the best of our knowledge this is the first study that analyzes the *dynamical* symmetry of biological rhythmic systems. We validate our methods in data from healthy human walking experiments. These methods are also applicable to robotic or biological locomotor behavior with approximately symmetric gait patterns.

## II. DATA SET

The system of interest is human treadmill walking. This data set is obtained for eight healthy young adult participants, at three different belt speeds (0.5, 1.0, and 1.5 m/s). Subjects walked with their arms crossed in all experiments. The Johns Hopkins Institutional Review Board approved all protocols and all subjects gave informed written consent before participating.

### A. The Kinematic Data

We placed infrared-emitting (IR) markers on subjects' left and right shoulder, hip, knee, ankle, and toe. The markers were tracked in 3D using Optotrak (Northern Digital) at 100 Hz. We reduce this data to the four sagittal plane angles on each side as illustrated in Figure 1. The raw angular data was smoothed with a fifth-order, zero-phase-lag (non-causal) Butterworth filter to remove measurement noise and ease angular velocity estimation. In order to estimate angular velocities, a central difference filter and another zero-phase-lag Butterworth filter was applied to the smoothed angular data. We assume that the smoothed angles (8) and angular velocities (8) form a

16 dimensional state space for walking. The state vector includes angles (rad),

$$\begin{aligned}\boldsymbol{\theta}_L(t) &= [\theta_{fL} \quad \theta_{aL} \quad \theta_{kL} \quad \theta_{hL}]^T, \\ \boldsymbol{\theta}_R(t) &= [\theta_{fR} \quad \theta_{aR} \quad \theta_{kR} \quad \theta_{hR}]^T, \\ \boldsymbol{\theta}(t) &= \begin{bmatrix} \boldsymbol{\theta}_L(t) \\ \boldsymbol{\theta}_R(t) \end{bmatrix}\end{aligned}\tag{1}$$

and angular velocities (rad/s),

$$\begin{aligned}\dot{\boldsymbol{\theta}}_L(t) &= [\dot{\theta}_{fL} \quad \dot{\theta}_{aL} \quad \dot{\theta}_{kL} \quad \dot{\theta}_{hL}]^T, \\ \dot{\boldsymbol{\theta}}_R(t) &= [\dot{\theta}_{fR} \quad \dot{\theta}_{aR} \quad \dot{\theta}_{kR} \quad \dot{\theta}_{hR}]^T, \\ \dot{\boldsymbol{\theta}}(t) &= \begin{bmatrix} \dot{\boldsymbol{\theta}}_L(t) \\ \dot{\boldsymbol{\theta}}_R(t) \end{bmatrix}.\end{aligned}\tag{2}$$

Subscripts  $f$ ,  $a$ ,  $k$ , and  $h$  stand for foot, ankle, knee, and hip, respectively.  $L$  and  $R$  mnemonically denote the left and right legs.

In order to analyze the data independently from the physical units, the state space was non-dimensionalized based on the time constant associated with pendular walking [18–21]:

$$\begin{aligned}\bar{\boldsymbol{\theta}} &= \boldsymbol{\theta} \\ \bar{\dot{\boldsymbol{\theta}}} &= \dot{\boldsymbol{\theta}} \sqrt{\frac{l_0}{g}},\end{aligned}\tag{3}$$

where the bar represents the corresponding non-dimensionalized variable,  $g$  is the gravitational acceleration, and  $l_0$  is the leg length of the subject which is estimated from the (IR) marker positions on right hip and ankle.

### B. Events and Section Data

The treadmill used in this study features a split belt<sup>1</sup> that mechanically decouples the vertical ground reaction forces caused by each foot. Each belt is instrumented with a separate load cell, facilitating the estimation of the timing of heel-strike events. We chose heel-strike events as Poincaré sections for the analyses.

Let  $t[k]$  be the detected times of heel-strike events, where  $k \in \mathcal{K} = \{1, 2, 3, \dots, k_{\max}\}$ , with  $k_{\max}$  being the total number of heel-strike events of both legs in one walking trial. For example, if the first heel-strike event ( $k = 1$ ) corresponds to the left leg, sets of odd ( $\mathcal{K}_L$ ) and even ( $\mathcal{K}_R$ ) integer indices from 1 to  $k_{\max}$  correspond to the left and right heel-strike events, respectively, such that  $\mathcal{K} = \mathcal{K}_L \cup \mathcal{K}_R$ . Over one stride of walking, there are two Poincaré sections of interest at heel-strike events. The measurement of the state vector at these Poincaré sections is given as follows:

$$\mathbf{z}[k] = \begin{bmatrix} \bar{\boldsymbol{\theta}}(t[k]) \\ \bar{\dot{\boldsymbol{\theta}}}(t[k]) \end{bmatrix}.\tag{4}$$

<sup>1</sup>While the belts of the treadmill can be driven at different speeds, this study addresses bilateral symmetry so both belts were driven at the same speed.

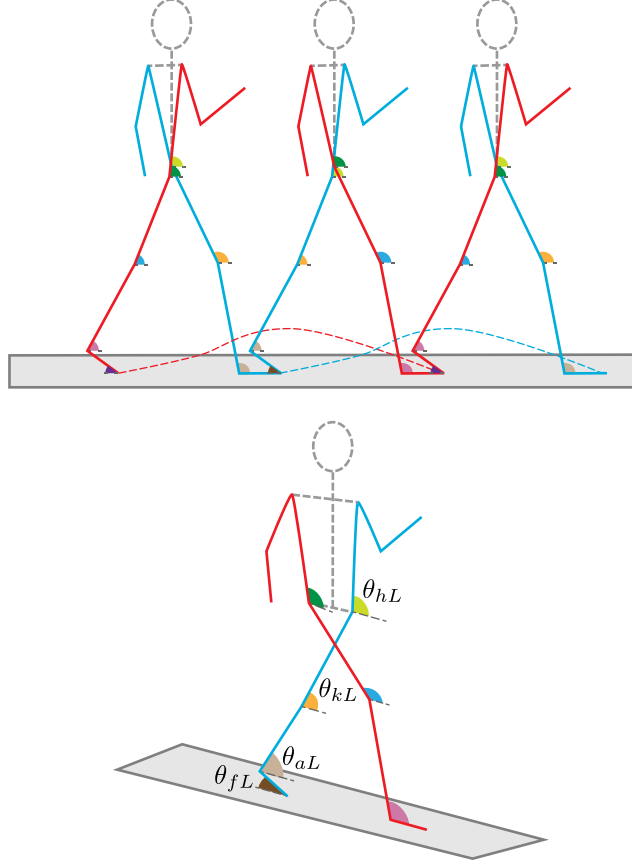


Fig. 1: Visualization of leg angle vector  $\theta$ . The left leg (blue) and right leg (red) alternate between stance and swing phase over the course of a stride. The variables  $\theta_{fL}$ ,  $\theta_{aL}$ ,  $\theta_{kL}$ , and  $\theta_{hL}$  correspond to the left foot, ankle, knee, and hip angles respectively. The corresponding right leg angles,  $\theta_{fR}$ ,  $\theta_{aR}$ ,  $\theta_{kR}$ , and  $\theta_{hR}$ , are not labeled. The 8 leg angles and their respective angular velocities form the 16-dimensional state vector.

During steady-state walking and in the absence of noise, the periodic orbit would remain on the limit cycle:

$$\begin{aligned} z[m] &= \mu_L, \quad \forall m \in \mathcal{K}_L \\ z[m'] &= \mu_R, \quad \forall m' \in \mathcal{K}_R \end{aligned} \quad (5)$$

where  $\mu_L$  and  $\mu_R$  are the fixed-points with respect to each of the two distinct Poincaré sections. Note that assuming bilateral symmetry implies that these two fixed points are identical up to a relabeling [11, 22–24]. This relabeling can be expressed as a linear mapping of right-heel-strike coordinates:

$$M : \begin{bmatrix} \bar{\theta}_L(t[k]) \\ \bar{\theta}_R(t[k]) \\ \bar{\dot{\theta}}_L(t[k]) \\ \bar{\dot{\theta}}_R(t[k]) \end{bmatrix} \mapsto \begin{bmatrix} \bar{\theta}_R(t[k]) \\ \bar{\theta}_L(t[k]) \\ \bar{\dot{\theta}}_R(t[k]) \\ \bar{\dot{\theta}}_L(t[k]) \end{bmatrix}, \quad \forall k \in \mathcal{K}_R, \quad (6)$$

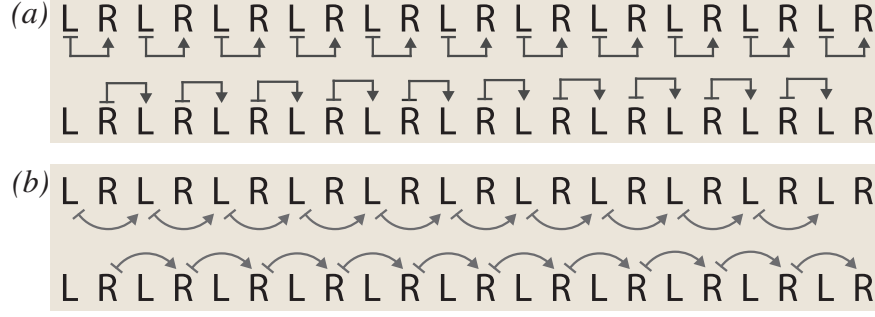


Fig. 2: Types of input–output pairs analyzed in this paper.  $L$  and  $R$  represent the Poincaré sections associated with heel-strike events of the left and right legs. (a) Left-to-right step maps (top) and right-to-right step maps (bottom). Step maps are denoted using straight arrows. (b) Left-to-left stride maps (top) and right-to-right stride maps (bottom). Stride maps and step maps are distinguished throughout the paper by shape (straight versus curved arrows, respectively).

where

$$M = \begin{bmatrix} 0 & I_{4 \times 4} & 0 & 0 \\ I_{4 \times 4} & 0 & 0 & 0 \\ 0 & 0 & 0 & I_{4 \times 4} \\ 0 & 0 & I_{4 \times 4} & 0 \end{bmatrix}. \quad (7)$$

As explained in Section I-A our approach to modeling human walking centers around fitting linear maps between Poincaré sections around the associated fixed points. First, we estimated the fixed points via

$$\begin{aligned} \hat{\mu}_L &= \frac{1}{|\mathcal{K}_L|} \sum_{k \in \mathcal{K}_L} z[k], \\ \hat{\mu}_R &= \frac{1}{|\mathcal{K}_R|} \sum_{k \in \mathcal{K}_R} z[k], \end{aligned} \quad (8)$$

where  $|\mathcal{K}_L|$  and  $|\mathcal{K}_R|$  denote the cardinality of sets  $\mathcal{K}_L$  and  $\mathcal{K}_R$  respectively. Note that *kinematic* asymmetry could be measured directly in terms of the difference between respective fixed points  $\hat{\mu}_L$  and  $\hat{\mu}_R$ ; while potentially of interest, the current paper focuses on *dynamical* asymmetry (measured in terms of the section maps), and thus we computed the residuals by subtracting the estimated fixed points from the section data:

$$\begin{aligned} \mathbf{q}_L[k] &= z[k] - \hat{\mu}_L, \quad k \in \mathcal{K}_L, \\ \mathbf{q}_R[k] &= z[k] - \hat{\mu}_R, \quad k \in \mathcal{K}_R. \end{aligned} \quad (9)$$

Section maps were estimated using these residuals. A section map from  $\mathbf{q}_L$  to the subsequent  $\mathbf{q}_R$  is denoted  $L \mapsto R$ . We fit two categories of section maps: step-to-step ( $L \mapsto R$  and  $R \mapsto L$ ) and stride-to-stride ( $L \mapsto L$  and  $R \mapsto R$ ). See Figure 2.

To fit the section maps for each category explained above, we stack all the appropriate residuals ( $\mathbf{q}_L$  and/or  $\mathbf{q}_R$ )

in matrices  $X$  (input) and  $Y$  (output):

$$X = [x_1, \dots, x_N]^T, \quad Y = [y_1, \dots, y_N]^T, \quad x_i, y_i \in \mathbb{R}^d \quad (10)$$

where  $x_i$  and  $y_i$  represent residuals ( $q$ ) from sections evaluated in the data. For example, to fit the  $L \mapsto R$  step-to-step map, one would set the columns of  $X$  and  $Y$  as follows:

$$\begin{aligned} x_1 &= q_L[1], & y_1 &= q_R[2], \\ x_2 &= q_L[3], & y_2 &= q_R[4], \\ &\vdots & &\vdots \\ x_N &= q_L[2N-1], & y_N &= q_R[2N]. \end{aligned} \quad (11)$$

The linear section maps are modeled as follows:

$$y_i = Ax_i + \delta_i, \quad \forall i, \quad (12)$$

$$Y = XA^T + \Delta, \quad (13)$$

where  $\delta_i$  is additive noise. The section map can be estimated via least squares:

$$\hat{A} = (X^\dagger Y)^T. \quad (14)$$

where  $X^\dagger$  is the MoorePenrose pseudoinverse of  $X$ .

### III. EXTENDING MONTE CARLO CROSS-VALIDATION

#### A. Classical Cross-Validation

Cross-validation (CV) involves fitting a model to a *training set* of input–output data, and validating the model by comparing its predictions on a complementary *test set* of input–output data. In classical CV, there exists  $n$  pairs of input–output data which are then split into a training (fitting) set ( $n_f$  pairs) and complementary test (validation) set ( $n_v = n - n_f$  pairs). The training set is used for model fitting. The fitted model is then applied to the inputs of the test set to generate output predictions; the error metric between the predicted and actual outputs is the *cross-validation error* (CVE). The CVE is used to evaluate the performance of the model. CV methods are commonly used for selecting models based on their predictive ability [25–27].

A critical question when using a CV method is how to split the data [25]. Assuming no replacement, there exists  $\binom{n}{n_v}$  different ways of splitting the data set. The most popular CV method, often called leave-one-out (LOOCV), uses  $n_v = 1$ , because it incurs the least computational cost. However, LOOCV is inconsistent (asymptotically biased) [25], and practically speaking, its performance is poor if the sample size is large. However for  $n_v \gg 1$  and  $(n - n_v) \gg 1$ , computing cross validation for all  $\binom{n}{n_v}$  possibilities can be computationally expensive. One way of decreasing the computational complexity is applying  $k$ -fold cross validation [28].

In  $k$ -fold CV, the data is initially split into  $k$  mutually exclusive, equal-sized subsets, and a LOO-type analysis is performed at the level of the subsets. Note that  $k$ -fold CV is computationally much more feasible than testing all

possible ways of splitting up the data, but there is a trade-off: picking small  $k$  increases the variance of the CVE estimate, while picking large  $k$ , which tends toward LOOCV, is biased for large sample sizes.

A common way to overcome the artificial trade-off between bias and variance imposed by  $k$ -fold CV, and still offer computational tractability, is Monte-Carlo cross validation (MCCV) [25]. MCCV randomly splits the data  $m$  times with fixed  $n_f$  and  $n_v$  (size of training and test sets respectively) over the  $m$  iterations. For each iteration the CVE is computed using the respective training and test sets; the overall CVE is estimated using the mean of these  $m$  CVEs. If  $\frac{n}{n_v} \ll m \ll \binom{n}{n_v}$ , MCCV estimates the CVE with a computationally feasible sample size, and with negligible variance compared to the estimate provided by  $k$ -fold CV. Also, since we fit the model more times ( $m \gg k$ ), MCCV provides a better mechanism to estimate model uncertainty compared to  $k$ -fold CV.

As mentioned before, the model being fit to input–output data in our case is a linear map. Suppose there are  $n$  pairs of input–output data,  $(x_i, y_i)$ , where  $i \in \mathcal{I} = \{1, 2, 3, \dots, n\}$ . Split this data into a training set  $\mathcal{F} \ni (x_f, y_f)$  comprising  $n_f$  pairs, and test set  $\mathcal{V} \ni (x_v, y_v)$  comprising  $n_v$  pairs. Define  $X_{\mathcal{F}}$  as the matrix whose rows are  $x_f^T$ , and define  $Y_{\mathcal{F}}$ ,  $X_{\mathcal{V}}$ , and  $Y_{\mathcal{V}}$  similarly. We use the following definition of CVE from  $\mathcal{F}$  to  $\mathcal{V}$ :

$$\text{CVE}_{\mathcal{F} \rightarrow \mathcal{V}} := \frac{\|Y_{\mathcal{V}} - X_{\mathcal{V}} A_{\mathcal{F}}^T\|^2}{\|Y_{\mathcal{V}}\|^2} \quad (15)$$

where  $\|\cdot\|$  denotes the Frobenius norm and

$$A_{\mathcal{F}} := \left( X_{\mathcal{F}}^\dagger Y_{\mathcal{F}} \right)^T \quad (16)$$

is the least-squares solution (14) given the training data  $\mathcal{F}$ .

### B. Extending Monte Carlo Cross-Validation

Here, we extend classical CV for systems that may exhibit discrete symmetry. We focus our discussion and notation on human walking but the methods developed may be applicable to other forms of locomotion that involve bilaterally symmetric gaits, such as walking and trotting—but not galloping [29]. In classical Monte Carlo CV, at each iteration one CVE is computed using (15), where as in our extended CV method we compute three types of CVEs. Each CVE computation uses the same test set, but the models are fit using three different training sets.

Each application of our extended CV method requires a “normal” set,  $\mathcal{N}$ , and an equal size “mirrored” set,  $\mathcal{M}$ . In this paper, we analyze four different  $(\mathcal{N}, \mathcal{M})$  pairs, which are generated using the input–output data types illustrated in Figure 2, i.e. step-to-step transitions ( $\{L \mapsto R\}$  and  $\{R \mapsto L\}$ ) and stride-to-stride transitions ( $\{L \mapsto L\}$  and  $\{R \mapsto R\}$ ). For example, if the normal data set comprises the left-to-right step transitions,  $\mathcal{N} = \{L \mapsto R\}$ , the associated mirrored dataset is  $\mathcal{M} = \{R \mapsto L\}$ . Similarly, for strides, if  $\mathcal{N} = \{L \mapsto L\}$  represents the set of all transitions from left heel strike to the subsequent left heel strike, then  $\mathcal{M} = \{R \mapsto R\}$  are the corresponding right-to-right transitions. All  $(\mathcal{N}, \mathcal{M})$  combinations are listed in Table I.

The normal and mirrored sets *each* include  $n$  mutually exclusive input–output pairs, denoted by  $(x_i, y_i) \in \mathcal{N}$  and  $(\hat{x}_i, \hat{y}_i) \in \mathcal{M}$ , respectively where  $i \in \mathcal{I} = \{1, 2, \dots, n\}$ . Each iteration of our extended CV methods randomly splits this index set  $\mathcal{I}$  into a training index set  $\mathcal{I}_f$  and test index set  $\mathcal{I}_v$  in a manner identical to classical CV:



$\mathcal{I}_f \cup \mathcal{I}_v = \mathcal{I}$  and  $\mathcal{I}_f \cap \mathcal{I}_v = \emptyset$ . The three types of CVE computations described below draw the test set from the normal dataset:

$$\mathcal{V} = \{(x_v, y_v) \in \mathcal{N} \mid v \in \mathcal{I}_v\}. \quad (17)$$

**Normal Cross Validation (NCV)** is the same as classical Monte Carlo CV, in that the test data are also drawn from  $\mathcal{N}$ :

$$\mathcal{F}_{\text{NCV}} = \{(x_f, y_f) \in \mathcal{N} \mid f \in \mathcal{I}_f\}. \quad (18)$$

This set is used for fitting the linear model  $A_{\mathcal{F}_{\text{NCV}}}$  using (16). Given  $A_{\mathcal{F}_{\text{NCV}}}$ , the CVE is computed on the common test set  $\mathcal{V}$  using (15). For NCV, the mirrored data  $\mathcal{M}$  is not used.

**Mirrored Cross Validation (MCV)** draws the training data from the mirrored dataset  $\mathcal{M}$ , using the same training index set  $\mathcal{I}_f$  as NCV:

$$\mathcal{F}_{\text{MCV}} = \{(\hat{x}_f, \hat{y}_f) \in \mathcal{M} \mid f \in \mathcal{I}_f\}. \quad (19)$$

As before, this set is used for computing the linear model  $A_{\mathcal{F}_{\text{MCV}}}$  using (16). The common test set  $\mathcal{V}$  is used for computing the CVE. In MCV we are using the “wrong” training data (mirrored), which will be critical for us to detect dynamical asymmetry in walking. Note that the size (and in fact the indices) of the training data in both MCV and NCV are the same.

**Combined Cross Validation (CCV)** uses training data that is the union of the training sets from NCV and MCV:

$$\mathcal{F}_{\text{CCV}} = \mathcal{F}_{\text{NCV}} \cup \mathcal{F}_{\text{MCV}}. \quad (20)$$

And, as before, this data is used to fit the linear model  $A_{\mathcal{F}_{\text{CCV}}}$  and the common test set  $\mathcal{V}$  is used for the CVE. Thus the model is fitted on data pooled from both  $\mathcal{N}$  and  $\mathcal{M}$ , while the test data remains the same. Note that CCV uses twice as much data for fitting as either NCV or MCV.

Figure 3 illustrates the set partitioning for one iteration of extended cross validation for a general dataset. Figure 4(a) illustrates one iteration of the extended cross validation algorithms on step data, where the normal dataset is  $\mathcal{N} = \{L \mapsto R\}$  and the mirrored dataset is  $\mathcal{M} = \{R \mapsto L\}$ . Figure 4(b) illustrates one iteration of the extended cross validation algorithms on stride data where  $\mathcal{N} = \{L \mapsto L\}$  and  $\mathcal{M} = \{R \mapsto R\}$ .

TABLE I: Catalog of normal,  $\mathcal{N}$ , and associated mirrored,  $\mathcal{M}$ , datasets combinations used in our extended CV analysis.

	$\mathcal{N}$	$\mathcal{M}$
Step	$\{L \mapsto R\}$	$\{R \mapsto L\}$
	$\{R \mapsto L\}$	$\{L \mapsto R\}$
Stride	$\{L \mapsto L\}$	$\{R \mapsto R\}$
	$\{R \mapsto R\}$	$\{L \mapsto L\}$

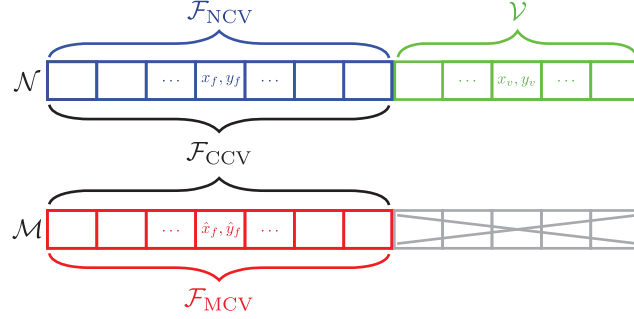


Fig. 3: Illustration of the subsets  $\mathcal{V}$ ,  $\mathcal{F}_{\text{NCV}}$ ,  $\mathcal{F}_{\text{MCV}}$ , and  $\mathcal{F}_{\text{CCV}}$  after random splitting during an iteration of extended cross validation methods. The normal dataset,  $\mathcal{N}$ , is randomly split into the normal training set  $\mathcal{F}_{\text{NCV}}$  and the common test set  $\mathcal{V}$ .  $\mathcal{F}_{\text{MCV}}$  shares the same indices as  $\mathcal{F}_{\text{NCV}}$  but is drawn from the mirrored dataset,  $\mathcal{M}$ . The training set for the CCV is simply the union of the other two training sets:  $\mathcal{F}_{\text{CCV}} = \mathcal{F}_{\text{NCV}} \cup \mathcal{F}_{\text{MCV}}$ . Note that the subset  $\mathcal{M} \setminus \mathcal{F}_{\text{MCV}}$  (greyed out) is not used in any of the three CV computations.

#### IV. RESULTS

As detailed in Section III-B our methods for analyzing dynamical symmetry in walking relies on Monte-Carlo sampling and cross-validation. We set the sample size of Monte-Carlo iterations for each application  $m = 1000$  based on pilot experiments that showed that increasing the sample size had a negligible effect on cross validation error. At each iteration, we withheld 20% ( $\frac{n_v}{n} = 0.2$ ) of the normal data set,  $\mathcal{N}$ , for cross validation. From the remaining data, we constructed the training sets for the three CV computations according to the procedure detailed in Section III-B.

##### A. Symmetric vs. Asymmetric Modeling

The question being addressed in this paper is not just the symmetry versus asymmetry of the dynamics of human walking, but also the statistical consequences of choosing one approach over the other. We applied our extended cross-validation method (Section III-B) to expose these consequences.

1) *Step Maps*: To apply our extended CV method to step-to-step transitions, we analyzed both combinations of normal and mirrored data:  $(\mathcal{N}, \mathcal{M}) = (\{L \mapsto R\}, \{R \mapsto L\})$  and  $(\mathcal{N}, \mathcal{M}) = (\{L \mapsto R\}, \{R \mapsto R\})$ ; see Table I. For each category of cross validation—NCV, MCV, and CCV—we averaged the errors for both combinations of  $(\mathcal{N}, \mathcal{M})$ .

The comparison between NCV and MCV is critical for statistically testing the symmetry of human walking. Since both NCV and MCV have training sets of the same size and MCV uses mirrored data, the difference in CVEs offer a direct measure of dynamical asymmetry. For a perfectly symmetric system we would expect NCV and MCV errors to be statistically indistinguishable. If there are asymmetries, we should observe higher MCV errors than NCV errors.

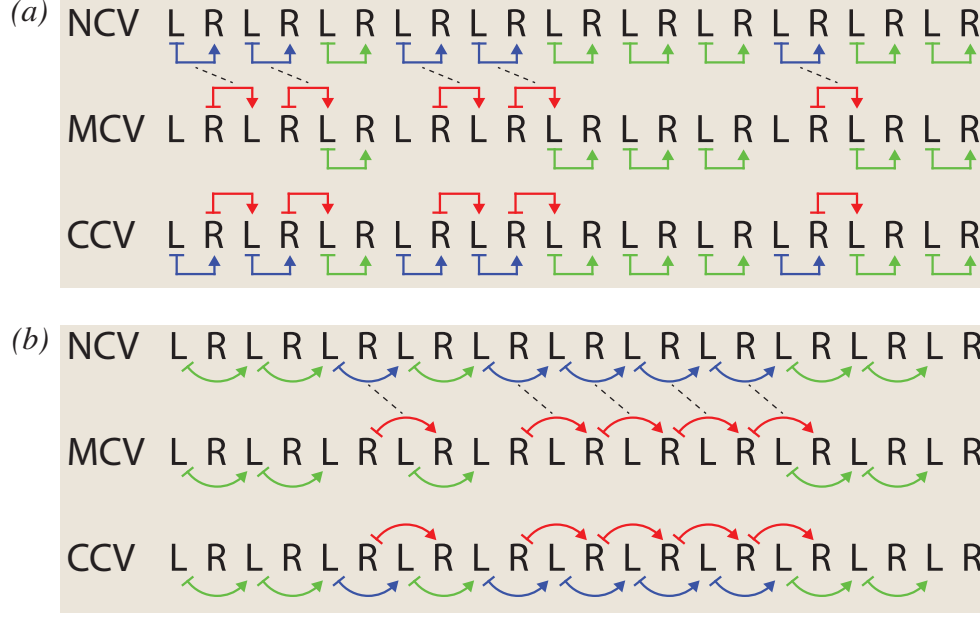


Fig. 4: Illustration of extended CV dataset partitioning. (a) For step-to-step data, the normal dataset ( $\mathcal{N}$ ) comprises all left-to-right step ordered pairs, whereas the mirrored dataset ( $\mathcal{M}$ ) comprises all right-to-left step ordered pairs. (b) For stride-to-stride data, the normal dataset ( $\mathcal{N}$ ) comprises all left-to-left stride ordered pairs, whereas the mirrored dataset ( $\mathcal{M}$ ) comprises all right-to-right stride ordered pairs. In both cases, for each iteration, a common test set ( $\mathcal{V}$ , green arrows), used for all CV methods, is randomly sampled from the normal dataset. The training sets, however, are unique to each method. NCV: the remainder of the normal dataset is used for training ( $\mathcal{F}_{\text{NCV}}$ , blue arrows). MCV: the training set ( $\mathcal{F}_{\text{MCV}}$ , red arrows) is obtained using the same indices (dashed lines) as for  $\mathcal{F}_{\text{NCV}}$ . CCV: the union of the test sets for NCV and MCV, comprise the combined training data ( $\mathcal{F}_{\text{CCV}} = \mathcal{F}_{\text{NCV}} \cup \mathcal{F}_{\text{MCV}}$ , red and blue arrows).

Figure 5(a) compares MCV and CCV errors to NCV error from step-to-step data. MCV errors are (statistically) significantly higher than NCV errors at all speeds ( $p_{1.5\text{m/s}} = 0.004$ ,  $p_{1\text{m/s}} = 0.008$  and  $p_{0.5\text{m/s}} = 0.004$ ; one-sided Wilcoxon rank-sign test). This shows that our data is indeed dynamically asymmetric between  $L \mapsto R$  and  $R \mapsto L$ .

However this comparison alone is not enough to address all concerns, because the main advantage of assuming symmetry is that we “double” the amount of data by combining  $\{L \mapsto R\}$  and  $\{R \mapsto L\}$  and fitting a single step return map. Indeed, the comparison of CCV and NCV errors illuminates a different perspective (Figure 5(a)). For speeds of 1.5 m/s and 1.0 m/s CCV and NCV errors were statistically indistinguishable ( $p_{1.5\text{m/s}} = 0.38$  and  $p_{1\text{m/s}} = 0.84$ ; Wilcoxon rank-sign test), suggesting that for these speeds, the predictive power of a model that assumes symmetry is just as great as one that embraces the asymmetry. More surprisingly, the average CCV error for the slowest speed tested was (statistically) significantly lower than the average NCV error ( $p_{0.5\text{m/s}} = 0.0039$ . Wilcoxon one-sided rank-sign test) for the slowest speed (0.5m/s). In other words, assuming symmetry (CCV)

produces a single step-to-step model that has greater predictive power than is achieved by refining the analysis to produce separate  $\{L \mapsto R\}$  and  $\{R \mapsto L\}$  step maps.

To summarize, even though there were distinguishable asymmetries in our data, we did not lose—and at the lowest speed, we gained—predictive power by assuming symmetry.

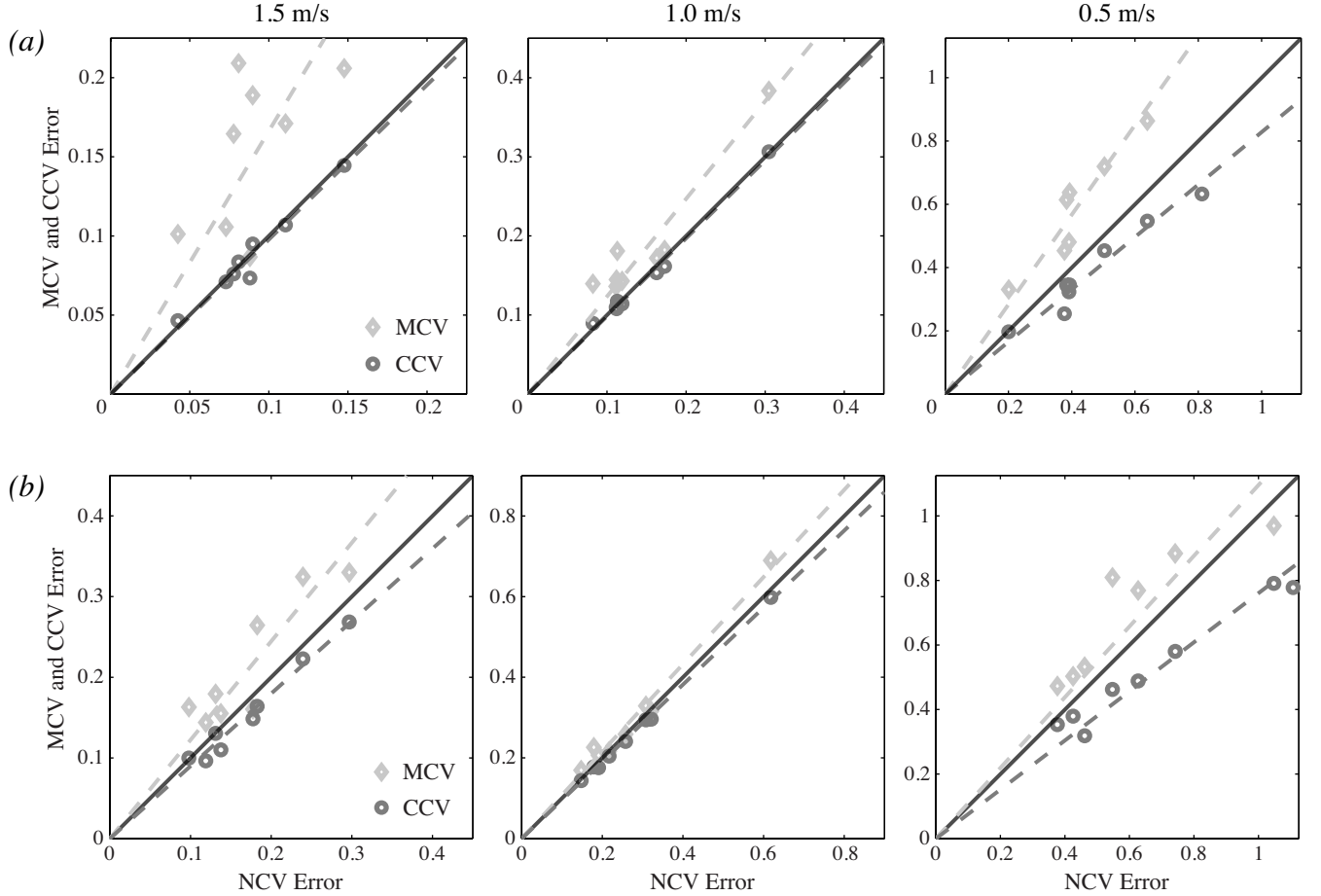


Fig. 5: Walking is asymmetric, but neglecting this by training a model on the combined data can nevertheless improve fitting. (a) Step-to-step maps. At all speeds, the mean mirrored cross validation errors (light grey diamonds) were significantly worse than for normal cross validation, indicating that steps were indeed asymmetric. Despite this left–right asymmetry, the mean combined cross validation errors were not significantly different than for normal cross validation at the two fastest walking speeds tested, and, more surprisingly, were actually *lower* at the slowest walking speed. The slopes of the fitted lines (dashed) determine the relative increase ( $m > 1$ ) or decrease ( $m < 1$ ) in CV error relative to the NCV error. (b) Stride-to-stride maps. By the same statistical measure, strides were also asymmetric at all speeds, but less substantially so. Moreover, the mean CCV error was lower than mean NCV error at all speeds.

2) *Stride Maps*: We analyzed the dynamical symmetry and the statistical consequences of symmetric modeling on the stride-to-stride transitions. Similar to before, we analyzed two different  $(\mathcal{N}, \mathcal{M})$  combinations,  $(\mathcal{N}, \mathcal{M}) = (\{L \mapsto L\}, \{R \mapsto R\})$  and  $(\mathcal{N}, \mathcal{M}) = (\{R \mapsto R\}, \{L \mapsto L\})$ ; see Table I. And again, for each category of cross validation, we averaged the CV errors for both combinations of normal and mirrored data. As in the previous section, we first compared NCV and MCV errors to test if the stride-to-stride data is statistically asymmetric. The NCV and CCV errors were also compared in order to compare the symmetric and asymmetric modeling approaches.

Figure 5(b) compares the MCV and CCV errors to NCV error for stride-to-stride data. MCV errors were higher (on average) than NCV errors for all speeds and these differences were statistically significant ( $p_{1.5m/s} = 0.0391$ ,  $p_{1m/s} = 0.0117$  and  $p_{0.5m/s} = 0.0039$ ; paired one-sided Wilcoxon rank-sign test). This shows that our data is dynamically asymmetric between  $L \mapsto L$  and  $R \mapsto R$ .

However, the comparison of NCV and CCV errors in stride-to-stride data is more striking than in the step-to-step case in that CCV errors were statistically significantly lower than the NCV errors at all three speeds ( $p_{1.5m/s} = 0.004$ ,  $p_{1m/s} = 0.012$  and  $p_{0.5m/s} = 0.004$ ; paired one-sided Wilcoxon rank-sign test).

Again, this analysis indicates that assuming symmetry produced models with more predictive power than were obtained by embracing the evident asymmetry in the stride-to-stride data.

3) *Model Uncertainty*: Even though CVEs in our analysis are powerful and suitable metrics for comparing the effectiveness of symmetric and asymmetric modeling approaches, we adopted another metric which we term *model uncertainty* similar to Madhav et al. [26]. We introduced this metric especially because of the observation that for step-to-step data CCV (symmetric approach) and NCV (asymmetric approach) errors at speeds 1.5 and 1.0 m/s are indistinguishable. This implies that both modeling approaches are equally powerful from the perspective of CVE. However, the parameters of the fitted section map model may exhibit greater variability for the asymmetric modeling approach since it uses less data for fitting.

In order to measure the uncertainty of the models we adopted following metric:

$$\Xi = \sum_{i=1}^d \sum_{j=1}^d \sigma_{ij}^2 \quad (21)$$

where  $\sigma_{ij}^2$  is the sample variance of  $a_{ij}$ , i.e. element at the  $i^{th}$  row and  $j^{th}$  column of the section map  $A_{\mathcal{F}}$  fit during Monte-Carlo iterations of the extended CV method. Symmetric model uncertainty was computed using the fitted matrix samples of the CCV method. Model uncertainties of the  $\{L \mapsto R\}$  and  $\{R \mapsto L\}$  (and  $\{L \mapsto R\}$  and  $\{R \mapsto L\}$ ) maps were averaged to have a single asymmetric model uncertainty for step maps (and stride maps).

We found that by neglecting asymmetry and fitting a single return map, there was a substantial reduction in model uncertainty for both the step-to-step and stride-to-stride data. See Figure 6. Thus, even though in a few cases, the CV errors were similar for NCV and CCV, the models produced using CCV (that is, neglecting asymmetry and pooling the data) are substantially less variable.

For step maps, assuming symmetry substantially lowers model uncertainty: we saw 56%, 54%, and 72% improvement with symmetric approach for speeds 1.5, 1.0 and 0.5 m/s respectively. All improvements were statistically significant ( $p = 0.0039$ , one-sided Wilcoxon signed-rank test). We observed the same trend with stride maps: 61%,

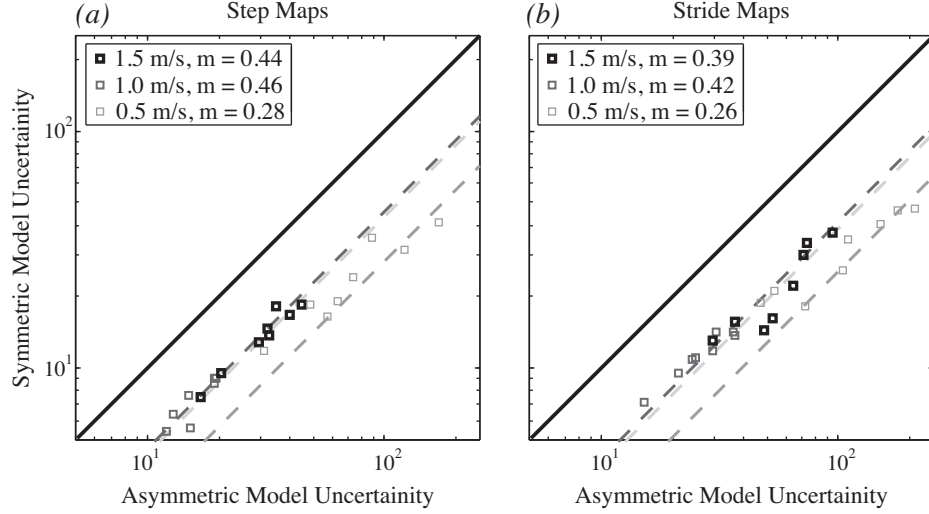


Fig. 6: Model uncertainty at all three speeds was lower when symmetry was assumed in both (A) step-to-step and (B) stride-to-stride maps. Each marker compares the model uncertainty with asymmetry and with symmetry of a single individual. Dashed line denotes the best fitted line (passing through the origin) to the comparison markers. The percentage improvement is given by  $(1 - m) \times 100$ , where  $m$  is the slope of the fitted line.

58%, and 74% improvement with symmetric approach for speeds 1.5, 1.0 and 0.5 m/s respectively ( $p = 0.0039$ , one-sided Wilcoxon signed-rank test). See Figure 6.

### B. Step Return Maps vs. Stride Return Maps

One of the advantages of assuming dynamical bilateral symmetry (i.e. neglecting asymmetry) is that one step becomes the fundamental period of the system: the mapping from step to step defines the return map of the dynamics. On the contrary, if we embrace the asymmetry, the stride becomes the fundamental period. The disadvantage of using stride-to-stride return maps compared to step-to-step maps is lowered signal-to-noise ratio due to the fact that stride maps reduce the temporal resolution. Stride-to-stride return maps have lower predictive power in the CV setting thus having higher CVEs.

In order to measure the loss of signal-to-noise ratio, we analyzed the CVEs by assuming symmetry and fitting return maps to both step and stride data. Specifically we compared the CCV errors of step and stride data in our method. In order to estimate CCV error of step return map we take the mean of CCV errors of  $\{L \mapsto R\}$  and  $\{R \mapsto L\}$ . Likewise, in order to estimate CCV error of stride return map, we take the mean of CCV errors of  $\{L \mapsto L\}$  and  $\{R \mapsto R\}$ .

The results illustrated in Figure 7 shows that there is a dramatic signal-to-noise ratio loss with stride-to-stride return maps and step-to-step return maps have more predictive power in the CV setting. CCV errors of stride return maps are significantly higher than the ones with step return maps: 79%, 87%, and 31% more CV error with stride return maps for speeds 1.5, 1.0, and 0.5 m/s respectively. The differences are statistically significant ( $p = 0.0039$ ,

one-sided Wilcoxon signed-rank test).

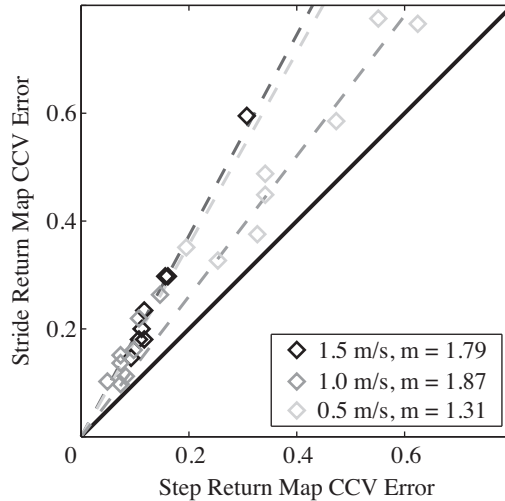


Fig. 7: Illustration of the CCV errors of step return maps and stride return maps. Each marker compares the CCV errors of step and stride return maps of a single individual. Dashed lines illustrate the best fitted lines (passing through the origin) to the comparison markers with  $m$  being the associated slope of the line.

## V. DISCUSSION

In this paper, we focused our attention on bilateral dynamic asymmetry in human walking. Specifically, we introduced a statistical framework based on applying cross validation techniques and fitting linear maps to the data associated with the heel strike events. Our statistical methods allowed us to examine the “wrongness” and “usefulness” of neglecting bilateral dynamic asymmetry.

We applied our methods to data obtained from eight different individuals and three different walking speeds. Based on the results obtained with this data set, we indeed observed that dynamical asymmetry in walking is significant and statistically distinguishable. Nevertheless, we showed that ignoring these asymmetries and modeling human walking dynamics as symmetric produces significantly more consistent models. Moreover, the predictive power of these symmetric models is higher than (or at worst equal to) their asymmetric counterparts. This shows that neglecting bilateral asymmetry—an inescapable characteristic of the human form—not only provides modeling convenience but, more importantly, produces better models in terms of consistency and predictive power. It is not only “OK” to neglect asymmetry; in some cases, it is better.

Even though we applied our methods to human walking data, they are directly applicable to a wide range of rhythmic dynamical systems in biology and robotics. Specifically we are interested in behaviors that exhibit alternating (out of phase) gait patterns but are symmetric via reversing the left–right axis for half the stride. This class includes bipedal walking, running, and sprinting [30, 31]; quadrupedal walking, trotting, and pacing [29, 32]; hexapedal alternating tripod gait [33, 34]; and even swimming [35, 36].

In the context of robotics, our methods can be used for diagnostics and calibration since symmetry is considered as a desired property in the design and development of robotic systems. Asymmetric robotic gaits can potentially increase energy expenditure, reduce performance, and introduce a steering bias, hindering the control and operation of the robot. It may be possible to eliminate this steering bias using existing gait adaptation methods [37,38] which, to date, requires external instrumentation and specialized arenas. However, our method relies on only internal kinematic measurements which are directly available in most robotic systems and so perhaps the methods presented in this paper can be used to develop a fast and effective calibration methods for field robotics.

On the biological side there is scientific value in investigating dynamical symmetry across species. Models of biological locomotion can be decomposed into two components: the mechanics of the locomotion (plant), and the neural feedback (controller) [39]. A “less wrong” model of the plant provides better understanding of the controller, and vice-versa [40,41]. The locomotor pattern of a behaving animal is the closed-loop interaction of the plant and controller. Investigating dynamical symmetry (or asymmetry) in the locomotor gait as well as symmetry (or asymmetry) of the kinematics allows us to better predict the structure of the corresponding neural controller.

With regard to human health in particular, our tools may be useful for understanding motor deficits during locomotion. Specifically, these methods provide an important extension to those that center on kinematic symmetry and its relations to human physiology [2, 8]. Individuals with damage to the musculoskeletal system or nervous system often use asymmetric kinematic walking patterns (e.g. amputees, stroke patients). The kinematic asymmetry can be in the amount of time standing on one leg versus the other, the extent of limb movements, or some combination. An understanding of the underlying dynamical asymmetry (or even symmetry) in these cases would provide more information about the nature of the deficit, and perhaps suggest new targets for focusing rehabilitation treatments.

Finally, an interesting extension of our methods would be analyzing *dynamical* asymmetry in gaits with categorically asymmetric steady-state kinematics such as quadrupedal galloping and bounding. The steady-state limit-cycles of such gaits are obviously asymmetric, but the dynamics around those limit-cycles may be symmetric (enough).

## VI. ACKNOWLEDGMENTS

This material is based upon work supported by the National Science Foundation (NSF) under grants 0845749 and 1230493 to N. J. Cowan and by the National Institutes of Health (NIH) under grant R01-HD048741 to A. J. Bastian.

## REFERENCES

- [1] Finnerty, J. R., Pang, K., Burton, P., Paulson, D. & Martindale, M. Q., 2004 Origins of bilateral symmetry: Hox and dpp expression in a sea anemone. *Science* **304**, 1335–1337. (doi:10.1126/science.1091946).
- [2] Reisman, D. S., Wityk, R., Silver, K. & Bastian, A. J., 2007 Locomotor adaptation on a split-belt treadmill can improve walking symmetry post-stroke. *Brain* **130**, 1861–1872. (doi:10.1093/brain/awm035).
- [3] Giakas, G. & Baltzopoulos, V., 1997 Time and frequency domain analysis of ground reaction forces during walking: an investigation of variability and symmetry. *Gait & Posture* **5**, 189–197. (doi:10.1016/S0966-6362(96)01083-1).
- [4] Karamanidis, K., Arampatzis, A. & Bruggemann, G. P., 2003 Symmetry and reproducibility of kinematic parameters during various running techniques. *Med. Sci. Sports. Exerc* **35**, 1009–1016. (doi:10.1249/01.MSS.0000069337.49567.F0).



- [5] Hsiao-Wecksler, E. T., Polk, J. D., Rosengren, K. S., Sosnoff, J. J. & Hong, S., 2010 A review of new analytic techniques for quantifying symmetry in locomotion. *Symmetry* **2**, 1135–1155. (doi:10.3390/sym2021135).
- [6] Muir, G. D. & Whishaw, I. Q., 1999 Complete locomotor recovery following corticospinal tract lesions: measurement of ground reaction forces during overground locomotion in rats. *Behav. Brain. Res* **103**, 45–53. (doi:10.1016/S0166-4328(99)00018-2).
- [7] Pourcelot, P., Audigie, F., Degueurce, C., Denoix, J. & Geiger, D., 1997 Kinematic symmetry index: a method for quantifying the horse locomotion symmetry using kinematic data. *Vet. Res.* **28**, 525.
- [8] Finley, J. M., Bastian, A. J. & Gottschall, J. S., 2013 Learning to be economical: the energy cost of walking tracks motor adaptation. *J. Physiol.* **591**, 1081–1095. (doi:10.1113/jphysiol.2012.245506).
- [9] Box, G. E. P. & Draper, N. R., 1987 *Empirical Model-Building and Response Surfaces*. Wiley.
- [10] Altendorfer, R., Koditschek, D. E. & Holmes, P., 2004 Stability analysis of legged locomotion models by symmetry-factored return maps. *Int. J. Robot. Res* **23**, 979–999. (doi:10.1177/0278364904047389).
- [11] Chevallereau, C., Grizzle, J. W. & Shih, C.-L., 2009 Asymptotically stable walking of a five-link underactuated 3-d bipedal robot. *IEEE Trans. Robot.* **25**, 37–50. (doi:10.1109/TRO.2008.2010366).
- [12] Ankarali, M. M. & Saranlı, U., 2010 Stride-to-stride energy regulation for robust self-stability of a torque-actuated dissipative spring-mass hopper. *Chaos* **20**. (doi:10.1063/1.3486803).
- [13] Seyfarth, A., Geyer, H. & Herr, H., 2003 Swing-leg retraction: a simple control model for stable running. *J. Exp. Biol* **206**, 2547–2555. (doi:10.1242/jeb.00463).
- [14] Holmes, P. J., Full, R. J., Koditschek, D. E. & Guckenheimer, J., 2006 The dynamics of legged locomotion: Models, analyses, and challenges. *SIAM Rev.* **48**, 207–304. (doi:10.1137/S0036144504445133).
- [15] Ankarali, M. M., Şen, H. T., De, A., Okamura, A. M. & Cowan, N. J., 2014 Haptic feedback enhances rhythmic motor control by reducing variability, not improving convergence rate. *J. Neurophysiol.* **111**, 1286–1299. (doi:10.1152/jn.00140.2013).
- [16] Guckenheimer, J. & Holmes, P., 1991 *Nonlinear Oscillations, Dynamical Systems, and Bifurcations of Vector Fields*. Springer.
- [17] Mattes, S. J., Martin, P. E. & Royer, T. D., 2000 Walking symmetry and energy cost in persons with unilateral transtibial amputations: matching prosthetic and intact limb inertial properties. *Arch. Phys. Med. Rehabil.* **81**, 561–568. (doi:10.1016/S0003-9993(00)90035-2).
- [18] Donelan, J. M., Kram, R. & Kuo, A. D., 2002 Mechanical work for step-to-step transitions is a major determinant of the metabolic cost of human walking. *J. Exp. Biol* **205**, 3717–3727.
- [19] Ankarali, M. & Saranlı, U., 2011 Control of underactuated planar pronking through an embedded spring-mass hopper template. *Auton. Robot.* **30**, 217–231. ISSN 0929-5593. (doi:10.1007/s10514-010-9216-x).
- [20] Saranlı, U., Arslan, O., Ankarali, M. M. & Morgul, O., 2010 Approximate analytic solutions to non-symmetric stance trajectories of the passive spring-loaded inverted pendulum with damping. *Nonlinear Dynam.* **62**, 729–742. (doi:10.1007/s11071-010-9757-8).
- [21] Blickhan, R. & Full, R. J., 1993 Similarity in multilegged locomotion: Bouncing like a monopode. *J. Comp. Physiol. A* **173**, 509–517. (doi:10.1007/BF00197760).
- [22] Westervelt, E., Grizzle, J. & Koditschek, D., 2003 Hybrid zero dynamics of planar biped walkers. *IEEE Trans. Automat. Contr.* **48**, 42–56. (doi:10.1109/TAC.2002.806653).
- [23] Duindam, V. & Stramigioli, S., 2009 Modeling and analysis of walking robots. In *Modeling and Control for Efficient Bipedal Walking Robots*, pp. 93–127. Springer.
- [24] Lee, J., Sponberg, S. N., Loh, O. Y., Lamperski, A. G., Full, R. J. & Cowan, N. J., 2008 Templates and anchors for antenna-based wall following in cockroaches and robots. *IEEE Trans. Robot.* **24**, 130–143. (doi:10.1109/TRO.2007.913981).
- [25] Shao, J., 1993 Linear model selection by cross-validation. *J. Am. Statist. Assoc.* **88**, 486–494.
- [26] Madhav, M. S., Stamper, S. A., Fortune, E. S. & Cowan, N. J., 2013 Closed-loop stabilization of the jamming avoidance response reveals its locally unstable and globally nonlinear dynamics. *J. Exp. Biol.* **216**, 4272–4284. (doi:10.1242/jeb.088922).
- [27] Rao, C. & Wu, Y., 2005 Linear model selection by cross-validation. *J. Statist. Plann. Inference* **128**, 231–240. (doi:10.1016/j.jspi.2003.10.004).
- [28] Kohavi, R., 1995 A study of cross-validation and bootstrap for accuracy estimation and model selection. In *Proc. of the Int. Joint Conf. on Artificial Intelligence*, volume 14, pp. 1137–1145.
- [29] Collins, J. J. & Stewart, I. N., 1993 Coupled nonlinear oscillators and the symmetries of animal gaits. *J. Nonlinear Science* **3**, 349–392. (doi:10.1007/BF02429870).

- [30] Mann, R. A. & Hagy, J., 1980 Biomechanics of walking, running, and sprinting. *Am. J. Sports Med.* **8**, 345–350. (doi:10.1177/036354658000800510).
- [31] Collins, S., Ruina, A., Tedrake, R. & Wisse, M., 2005 Efficient bipedal robots based on passive-dynamic walkers. *Science* **307**, 1082–5. (doi:10.1126/science.1107799).
- [32] Buehler, M., Battaglia, R., Cocosco, A., Hawker, G., Sarkis, J. & Yamazaki, K., 1998 Scout: A simple quadruped that walks, climbs, and runs. In *IEEE International Conference on Robotics and Automation*, volume 2, pp. 1707–1712. IEEE.
- [33] Full, R. J. & Tu, M. S., 1990 Mechanics of six-legged runners. *J. Exp. Biol.* **148**, 129–146.
- [34] Saranli, U., Buehler, M. & Koditschek, D. E., 2001 RHex: A simple and highly mobile hexapod robot. *Int. J. Robot. Res.* **20**, 616–631. (doi:10.1177/02783640122067570).
- [35] Sfakiotakis, M., Lane, D. M. & Davies, J. B. C., 1999 Review of fish swimming modes for aquatic locomotion. *IEEE J. Ocean. Eng.* **24**, 237–252. (doi:10.1109/48.757275).
- [36] Ijspeert, A. J., Crespi, A., Ryczko, D. & Cabelguen, J.-M., 2007 From swimming to walking with a salamander robot driven by a spinal cord model. *Science* **315**, 1416–1420. (doi:10.1126/science.1138353).
- [37] Weingarten, J., Lopes, G. A. D., Buehler, M., Groff, R. E. & Koditschek, D., 2004 Automated gait adaptation for legged robots. In *IEEE International Conference on Robotics and Automation*, volume 3, pp. 2153–2158. (doi:10.1109/ROBOT.2004.1307381).
- [38] Galloway, K., Clark, J., Yim, M. & Koditschek, D., 2011 Experimental investigations into the role of passive variable compliant legs for dynamic robotic locomotion. In *IEEE International Conference on Robotics and Automation*, pp. 1243–1249. (doi:10.1109/ICRA.2011.5979941).
- [39] Roth, E., Sponberg, S. & Cowan, N. J., 2014 A comparative approach to closed-loop computation. *Curr. Opin. Neurobiol.* **25**, 54–62. (doi:10.1016/j.conb.2013.11.005).
- [40] Cowan, N. J. & Fortune, E. S., 2007 The critical role of locomotion mechanics in decoding sensory systems. *J. Neurosci.* **27**, 1123–1128. (doi:10.1523/JNEUROSCI.4198-06.2007).
- [41] Cowan, N. J., Ankarali, M. M., Dyhr, J. P., Madhav, M. S., Roth, E., Sefati, S., Sponberg, S., Stamper, S. A., Fortune, E. S. & Daniel, T. L., 2014 Feedback control as a framework for understanding tradeoffs in biology. *Integr. Comp. Biol.* ISSN 1540-7063. (doi:10.1093/icb/icu050).